Commercially-Hosted Payloads for Debris Monitoring and Mission Assurance in GEO

James R. Shell
US Air Force, Space Innovation and Development Center
24 Talon Way, Schriever AFB, CO 80912

ABSTRACT

Space capabilities derived from the geosynchronous orbit (GEO) are unique and difficult to replicate in other orbital regions. Therefore, a premium is placed on the preservation of the GEO. An accurate understanding of the efficacy of debris mitigation measures is essential. Evidence seems to indicate retired systems in disposal orbits are shedding materials that transit the GEO region. In addition, there are concerns that counter-space activities could threaten critical services enabled by GEO-based systems. Commercially hosted optical payloads are a cost-effective approach to monitor the debris environment and they may deter possible interference with GEO-based operations. Use of commercially hosted payloads is highly synergistic with the United States National Space Policy which calls for increased commercial involvement, as well as international debris monitoring and space situational awareness data sharing.

The detection performance of modest GEO-based payloads is significant when compared to low earth orbit based and ground-based telescopes. The geometry and persistence enabled by these payload systems have unique advantages. A parametric performance analysis is made as a function of optical system design variables. The debris detection capabilities for the GEO environment are described, and a notional architecture proposed and examined.

1 INTRODUCTION

Commercially-hosted space situational awareness (SSA) payloads concurrently satisfy numerous technical and political objectives. The 2010 US National Space Policy[1] emphasizes leveraging commercial capabilities and expanding space situational awareness and orbital debris monitoring. Geostationary communications satellites are particularly attractive, which may be used as hosts for optical telescope payloads directed down the Geostationary Orbit (GEO). This persistent coverage may also provide a capability to "detect, identify, and attribute actions in space that are contrary to responsible use," as stated in the National Space Policy. The US National Security Space Strategy[2] also emphasizes commercial partnerships in areas which would improve resiliency. The concept of commercially-hosted GEO-based SSA sensors is not new,[3] but now is an optimal time to leverage this potentially low-cost path to enable new capability. The newly established Hosted Payload Alliance[4] also provides an efficient interface for helping to plan and integrate such payloads.

> *"The United States shall…develop, maintain, and use space situational awareness (SSA) information from commercial, civil, and national security sources to detect, identify, and attribute actions in space that are contrary to responsible use and the long-term sustainability of the space environment"* **US National Space Policy, June 2010**
>
> *"Strategic partnerships with commercial firms will be pursued in areas that both stabilize costs and improve the resilience of space architectures upon which we rely."* **US National Security Space Strategy, January 2011**

In situ GEO sensors would significantly expand the knowledge of the small debris population in GEO, which are difficult objects to detect from ground-based or LEO-based sensors. A better understanding of this class of GEO debris objects could lead to an improved understanding of debris sources and hence inform mitigation practices.[5] The geometric diversity provided from GEO sensors is also complementary, as they provide solar illumination conditions ~90 degrees different relative to ground- and LEO-based sensors. This same geometric diversity also enables improved orbit determination when combined with other angles-only metric observations.[6] This effort

examines the performance of such sensors, investigating detection sensitivities and optical design options for payloads that are relatively low cost and minimally intrusive to the host.

2 GEO DEBRIS ENVIRONMENT

Currently, there are approximately 1000 GEO objects in the space catalog maintained by the United States and available through www.space-track.org. The GEO region is defined in various ways, with a common definition being an altitude ranging from 35,786 km (GEO) ± 200 km and a latitude range of ±15 degrees. The debris monitoring area of interest however, is larger than the GEO region, and includes the GEO "disposal" orbits at higher altitudes, having a minimum perigee typically 235 km above GEO. Ground-based telescope surveys indicate that at the 10 cm and larger object size, there are some 3200 GEO objects.[7,8] Furthermore, a new class of objects having high area-to-mass ratios (or "HAMR" objects) has been discovered,[9] with unique orbital properties due to the high relative solar radiation pressure perturbations. Such objects, though presumably originating in the GEO region or GEO disposal orbits, may have inclinations well exceeding the typical 15 degree limit naturally incurred from earth oblateness and solar-luni gravitational perturbations. Similarly, high eccentricities are possible with these objects.[10] The nature of the GEO debris population for objects smaller than 10 cm is highly uncertain,[11] but new survey results[12] reinforce the notion of an exponentially increasing population similar to that observed in LEO.

The debris collision risks at GEO are actually very low, with debris spatial densities orders of magnitude below those in some LEO orbits. Furthermore, the relative impact velocities are reduced, resulting in damage thresholds which are lower in GEO for equivalent sized LEO objects. The collision risk is also non-uniform, with the highest collision probabilities occurring around the geopotential wells.[13] Perhaps most telling of the risk, insurers have no appreciable near-term concern for debris collisions at GEO.[14] However, the lack of a "cleansing" mechanism in GEO, such as atmospheric drag in LEO, urges careful consideration of the long-term preservation of this unique orbit. Independent of debris collision risks, the potential to deter hostile actions in GEO is also beneficial.

A brief description of debris optical signatures is provided, a necessary input to model the performance of these sensors. Debris optical signatures may be approximated using spherical objects, resulting in a visual magnitude signature of

$$m_{obj} = m_{sun} - 2.5\log\left[\frac{d^2}{R^2}\cdot\left(\frac{\rho_{spec}}{4} + \rho_{diff}\, p_{diff}(\psi)\right)\right], \tag{1}$$

where d is the object diameter, R is the range and ρ_{spec} and ρ_{diff} are the specular and diffuse reflection components. Finally, the visual magnitude of the sun, m_{sun}, is a constant term equal to -26.73. The term p_{diff} is the solar phase angle function, responsible for objects being brighter when the illumination source and the observer or sensor angular separation, ψ, is minimum (*i.e.*, for a full moon, $\psi = 0°$, and for a half moon, $\psi = 90°$). The phase angle function for a diffuse sphere is

$$p_{diff}(\psi) = \frac{2}{3\pi}\cdot\left[\sin(\psi) + (\pi - \psi)\cos(\psi)\right].^{15} \tag{2}$$

Conversion from visual magnitude to engineering radiometric units is given by

$$E_{RSO} = 5.6\times10^{10}\cdot10^{-0.4\cdot m_{obj}} \quad [\text{photons/s/m}^2] \tag{3}$$

which considers the solar irradiance spectral content, along with a typical silicon detector response curve as a function of wavelength.

3 OPTICAL PAYLOAD PERFORMANCE

For cost minimization, it is desirable for the optical telescope to remain in a fixed position relative to their commercial host, eliminating the complexity of mechanical components. To first order, two telescopes per host would be oriented along the GEO belt, one in the positive velocity direction and one in the negative. Previous work has quantified the detection performance of fixed-staring optical surveillance telescopes, and will not be repeated in great detail here.[16] Only the key equations describing the detection performance is discussed.

A signal-to-noise (SNR) ratio greater than six is typically desired to achieve reasonable detection performance within a single image frame without introducing too many false alarms. Multiple frame processing can enable significant reduction of this threshold with advanced track before detect dim target algorithms, but for simplicity, a $SNR > 6$ is used. For space-based sensors, it is noted that cosmic ray impacts and other artifacts introduce single frame detection anomalies, which may be reliably eliminated by multiple frame processing. The SNR is defined as the number of signal photoelectrons, e_s, divided by the square root of the background radiance-produced photoelectrons, e_b, added to the square of the detector noise electrons, e_n, or

$$SNR = \frac{e_s}{\sqrt{e_b + e_n^{\,2}}} \cdot \tag{4}$$

The number of signal photoelectrons are a product of the resident space object signature, E_{RSO}, aperture area of the telescope, A, the net transmittance through the optical system, τ, (which is inclusive of obscurations), the quantum efficiency of the detector, QE, and the signal integration time, t_{sig}. The resulting expression, assuming the signal point spread function is contained within a single pixel, is provided by Equation 2.

$$e_s = QE \cdot \tau \cdot A \cdot E_{RSO} \cdot t_{sig} \ . \ \text{[photoelectrons]} \tag{5}$$

However, the signal integration time for a fixed staring sensor is limited by the debris object angular rate, ω. Once the object transits more than a single pixel, or streaks, there is no additional signal energy accumulation. Instead, the background photoelectrons continue to accumulate thus lowering the SNR. The angular extent of a single pixel, known as the instantaneous field of view or IFOV, is the pixel size divided by the focal length, or x/f. The IFOV will be represented by μ. Therefore, the maximum integration time in terms of optical system variables is

$$Max(t_{sig}) = \frac{x}{f \cdot \omega} \cdot \ \text{[sec]} \tag{6}$$

Having quantified the signal, an expression for the background noise photoelectrons is needed. Many of the same variables responsible for the signal photoelectrons also directly impact the background photoelectrons, such as aperture area, net optical transmittance and detector quantum efficiency. The expression for the number of photogenerated electrons from the background radiance is given by

$$e_b = QE \cdot \tau \cdot L_b \cdot A \cdot \mu^2 \cdot t \quad , \ \text{[photoelectrons]} \tag{7}$$

where L_b is the extended radiance from the background. A detailed treatment also includes a small dependency upon the f number of the optical system, but Equation 7 is adequate for this treatment and errs on the side of conservative system performance.

Inserting the expressions for the signal and background radiance photoelectrons into SNR equation results in

$$SNR = \frac{QE \cdot \tau \cdot A \cdot \tau_{atm} \cdot E_{RSO} \cdot t_{sig}}{\sqrt{\left(QE \cdot \tau \cdot L_b \cdot A \cdot \mu^2 \cdot t\right) + e_n^{\,2}}} \cdot \tag{8}$$

For cases where the background radiance is the dominant noise term, or $e_b >> e_n^2$, it may be further shown that the optimal SNR can be simplified to

$$SNR = \sqrt{QE \cdot \tau \cdot A}\, \frac{E_{RSO}}{\sqrt{L_b \cdot \omega \cdot \mu}} \cdot \tag{9}$$

4 GEOMETRY AND GEO DEBRIS KINEMATICS

Having determined expressions for debris signatures and optical telescope detection performance, it is now necessary to investigate both the geometry and motion of debris objects. As seen in the previously developed equations, both range and angular rates directly impact the performance.

Figure 1 illustrates the geometry, and the variables that will be used to derive expressions which may be used in the SNR equation.

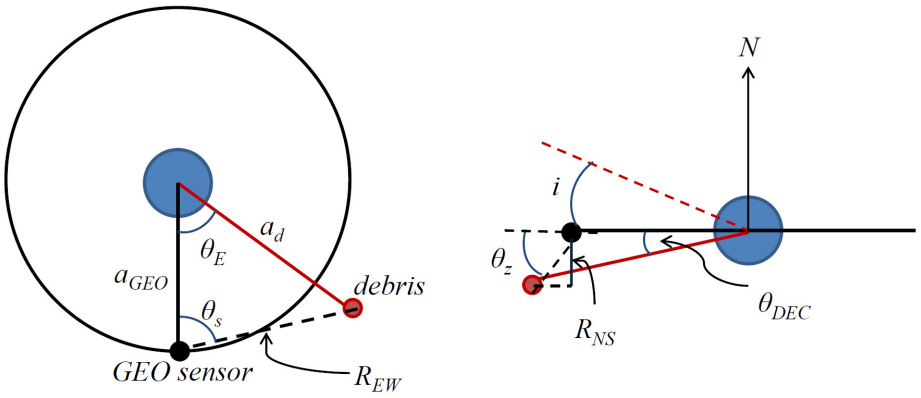

Figure 1 The geometry of the GEO-based observation of other objects is illustrated. On the left is the view from above the GEO orbital plane, while the right provides a side view looking along the GEO plane.

4.1 Range

First, the ranges are considered. The angle θ_E is used as the earth-centered angle between the geostationary observational platform and the debris object with semi-major axis of a_d. The east-west range (R_{EW}) to the debris object within the geostationary orbital plane is provided by the law of cosines and given by

$$R_{EW}(\theta_E, a_d) = \sqrt{a_{GEO}^{\ 2} + a_d^{\ 2} - 2 \cdot a_{GEO} \cdot a_d \cdot \cos(\theta_E)}\,, \tag{10}$$

where a_{GEO} is the geostationary semi-major axis, or 41,258 km. The north-south range component is given by

$$R_{NS}(\theta_{DEC}, a_d) = a_d \cdot \sin(\theta_{DEC})\,. \tag{11}$$

The total range to the object is therefore given by

$$R(\theta_{DEC}, \theta_E, a_d) = \sqrt{R_{NS}^{\ 2} + R_{EW}^{\ 2}}\,. \tag{12}$$

Figure 2 illustrates the range as a function of θ_{DEC} and θ_E.

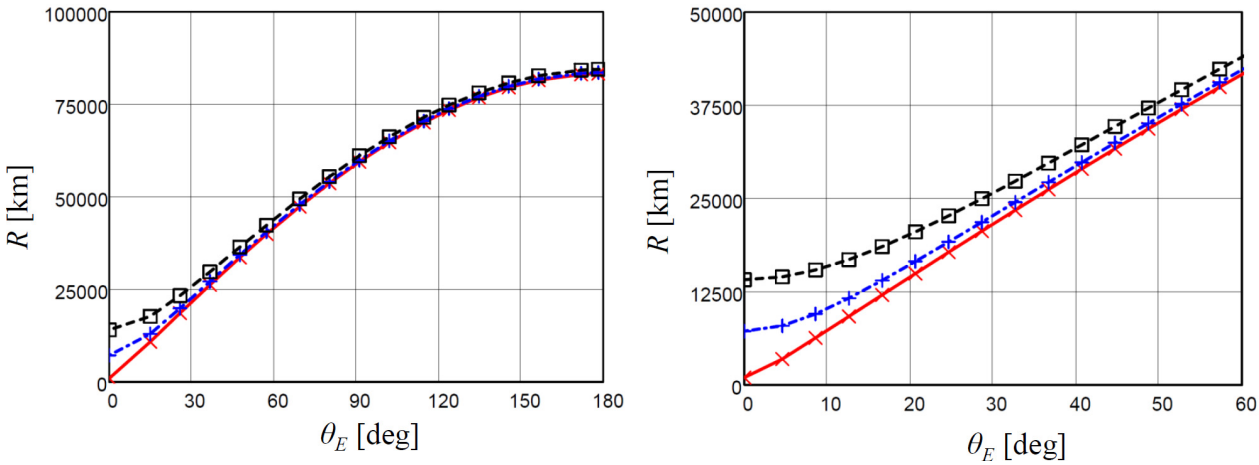

Figure 2 The range to other GEO objects (y-axis, km) as a function of the "belt angle", θ_E (x-axis, degrees). The ×, +, and □ lines correspond to a declination angles (θ_{DEC}) of 0°, 10°, and 20°. At left, the full range around the belt is shown, while the figure on the right is restricted to $\theta_E < 60°$.

4.2 Relative Angular Velocity

Derivation of the relative motion is a bit more complex. Circular orbits will be assumed for all objects, and the commercial host for the payload will be assumed to stay in a geostationary orbit, or one with no inclination. The relative motion is comprised of an east-west or "EW" component due to an altitude (semi-major axis) difference and north-south or "NS" motion due to object inclination.

The absolute NS velocity component may be shown to equal

$$vel_{NS}(i, a_d, \theta_{DEC}) = \cos(\theta_z) \frac{2 \cdot \pi \cdot i \cdot a_d}{P} \cdot \cos\left[\frac{\pi \cdot \theta_{DEC}}{2 \cdot i}\right], \tag{13}$$

where i is the inclination of the debris object orbit, and θ_z is the look angle out of the GEO plane (ref Figure 1). It is defined according to

$$\theta_z = \sin^{-1}\left[\frac{R_{NS}}{R}\right],$$

and P is the orbital period or

$$P(a_d) = \sqrt{\frac{4 \cdot \pi^2 \cdot a_d^{\,3}}{\mu}}. \tag{14}$$

where μ is the gravitational parameter (3.986 x 10^5 km^3/s^2). The maximum NS velocity component is achieved while crossing the GEO orbital plane ($\theta_{DEC} = 0°$), and increases with the orbit inclination, i. This behavior is shown in Figure 3.

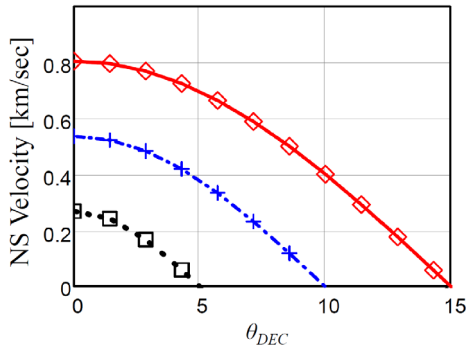

Figure 3 The north south velocity of GEO objects as a function θ_{DEC} for inclinations of 5°, 10° and 15° or □, + and ◊, respectively.

For the east-west (EW) velocity component, it may be shown that the relative orthogonal orbital velocity component in the EW plane is given by

$$vel_{EW}(\theta_E, a_d) = \cos(\theta_s) \cdot \left[a_d \cdot \cos(\theta_s) - a_{GEO} \cdot \sin(\theta_s)^2\right] \cdot \left[\sqrt{\frac{\mu}{a_d^{\,3}}} - \sqrt{\frac{\mu}{a_{GEO}^{\,3}}}\right], \tag{15}$$

where θ_s is the angle to the debris object relative to the nadir of the geostationary platform (ref Figure 1). θ_s is given as

$$\theta_s(\theta_E, a_d) = \sin^{-1}\left[\frac{a_d \cdot \sin(\theta_E)}{R(\theta_E, a_d)}\right]. \tag{16}$$

Having determined the individual EW and NS velocity components (Equations 13 and 15), the angular rates of objects relative to the stationary GEO host may be obtained. The angular rate, ω, is obtained by adding the individual velocity components in quadrature, and dividing by the range, or,

$$\varpi(\theta_E, a_d, i, \theta_{DEC}) = \sqrt{\varpi_{EW}(\theta_E, a_d)^2 + \varpi_{NS}(i, a_d, \theta_{DEC})^2} = \frac{\sqrt{vel_{EW}(\theta_E, a_d)^2 + vel_{NS}(i, a_d, \theta_{DEC})^2}}{R(\theta_{DEC}, \theta_E, a_d)}. \quad (17)$$

This equation is further explored and visualized in Figure 4, where it is noted that for objects 2 degrees away in the GEO belt that relative angular rates above 100 asec/sec are possible for objects with 15° of inclination. Similarly, for objects 45 degrees away in the GEO belt, maximum angular rates of only ~5 asec/sec are obtained, or similar to that observed from the ground due to the similar ranges involved, and the fact that NS motion dominates.

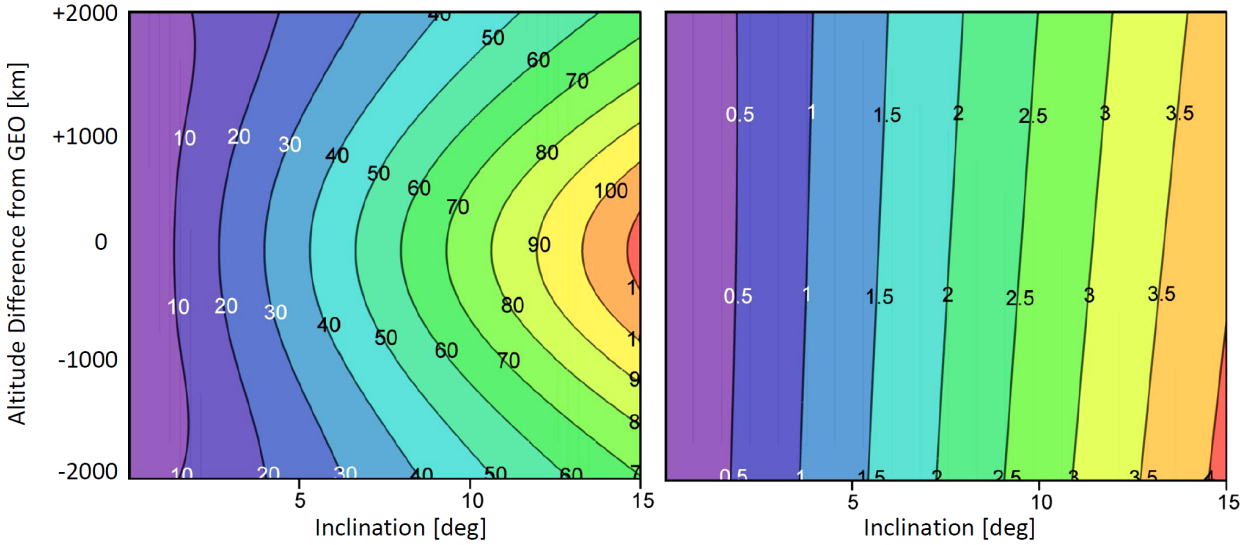

Figure 4 The apparent angular rate of objects as seen from a GEO platform as they cross the GEO plane (or $\theta_{DEC} = 0°$) for objects 2 degrees away in the GEO belt, ($\theta_E = 2°$, left) and 60 degrees away in the GEO belt ($\theta_E = 60°$, right) as a function of inclination (x-axis) and altitude difference from GEO (y-axis).

5 ARCHITECTURE PERFORMANCE

For this section, the detection performance and the geometric placement and coverage of GEO is examined.

5.1 Object detection performance

The optical performance equations developed in Section 3 are now combined with the range and angular rate knowledge developed in Section 4 to understand the performance of candidate optical designs.

For this exercise, performance is parametrically investigated, with the primary independent variable being the optical system aperture diameter, as this is closely tied to driving cost of the payload and the size, weight and power (SWAP) requirements of the commercial host. A back-illuminated silicon CCD is used, with parameters typical of a commercial off-the-shelf (COTS) detector. The baseline system and conditions used for the analysis is shown in Table 1.

Table 1 Optical system design parameters used in the performance investigation.

Subsystem	Parameter and units	Variable	Value
CCD	CCD Pixel Size [μm]	x	15
	CCD QE	QE	0.7
	Read Noise [electrons]	e_n	5
Optical System	Optical system throughput	τ	0.7
	Optical system focal ratio	f / d	1.2
Object	RSO Reflectance (diffuse)	ρ_{diff}	0.2
	Solar Phase Angle [deg]	ψ	90
Environment	Background radiance [M_v / asec^2]	L_b	21.5

The system performance is investigated at two different ranges in the GEO belt, corresponding to the ranges of the two previously investigated angular rates (Figure 4) or 2° and 60° away in the belt. Here the optimal integration time is used, thus establishing the best case performance for the system. The results are depicted in Figure 5.

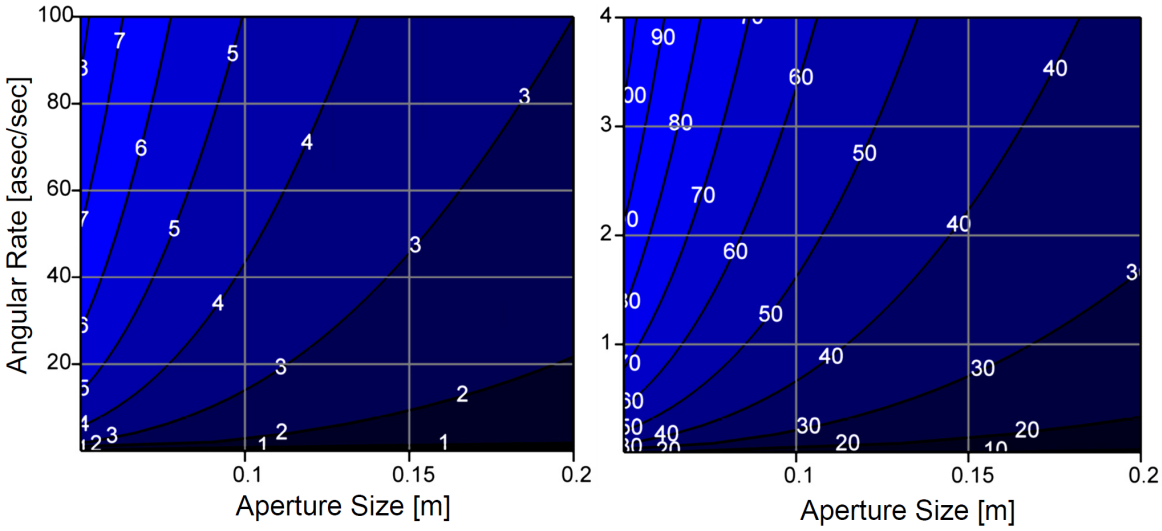

Figure 5 The minimum object size detected (units of cm) as a function of telescope aperture size (x-axis) and angular rate (y-axis). At left is for objects 2 degrees away in GEO (R = 1472 km) and right 60 degrees away in GEO (R = 42,160 km).

It is seen for the nearby, 2° away in GEO case (Figure 5, left), that a 10 cm aperture can provide detection of object sizes less than 5 cm. For the longer range objects 60° away in GEO, detection of objects less than 70 cm are possible for the 10 cm aperture. The range of angular rates shown in Figure 5 are approximately up to what a 15° object would present at its highest rate, or as it crosses the GEO belt (θ_{DEC} = 0°).

It is reminded that the maximum object angular rate is being considered, and that at the north-south "turnaround points", or when inclination is equal to the declination angle, that the relative north-south angular rates instantaneously go to zero. For objects with minimal altitude difference (or sufficient range), the east-west angular rate component is also minimal, thus an improved detection threshold is enabled via longer integration times.

5.2 Payload placement and resulting GEO belt coverage

Now the question is asked, what is the ideal orientation to place such systems in, and what do varying fields of view provide? One apparent answer is to place the telescopes looking directly down the belt in either direction from the host, or in the positive and negative velocity vector direction. However, such placement affords only a limited viewing range of GEO, as seen from an investigation of the geometries.

A viewing angle canted "inward" toward the GEO belt provides better coverage of the GEO region, as every angle increment translates to twice that angle around the GEO belt. In other words, looking one degree off the velocity vector from a GEO platform intersects the GEO belt two degrees, five degrees translates to a GEO angle of 10 degrees, etc.

Wide field of view systems are desired to provide broad area coverage, but this comes at the sacrifice of metric accuracy. For instance, the 10 cm aperture, *f*/1.2 system coupled with 15 μm pixels, or that used in the previous example to determine performance, provides an IFOV of 25.8 asec. While metric performance is usually better than the IFOV, it is still very poor compared to typical values of ground-based systems observing GEO, i.e., 4 asec or better. However, one must consider a few factors—the ranges involved with GEO-based sensors may result in a comparable overall absolute distance errors with these larger IFOVs, and perhaps more important, the orthogonal viewing conditions compared to ground and LEO-based sensors.

For illustrative purposes, a notional architecture is suggested providing persistent GEO coverage. Six commercial hosts are used, with each having two, 10 cm telescopes of the aforementioned design. An idealized spacing will be considered, such that the hosts are equally spaced 60° apart (acknowledged as not being realistic given the opportunistic nature of hosted payloads). Each telescope has a field of view of 20°, which translates to a focal array size of ~42 mm, and pushes the demands of the optical system to maintain performance at the edge of the field. The optical axis of telescopes are pointed 20° inward, such that the field of view spans 10-30° relative to the velocity (and anti-velocity) vector, or equivalent to sampling GEO belt angles of 20-60° away from the host system. This architecture is illustrated in Figure 6, where the geometric coverage relative to the current GEO object catalog is seen.

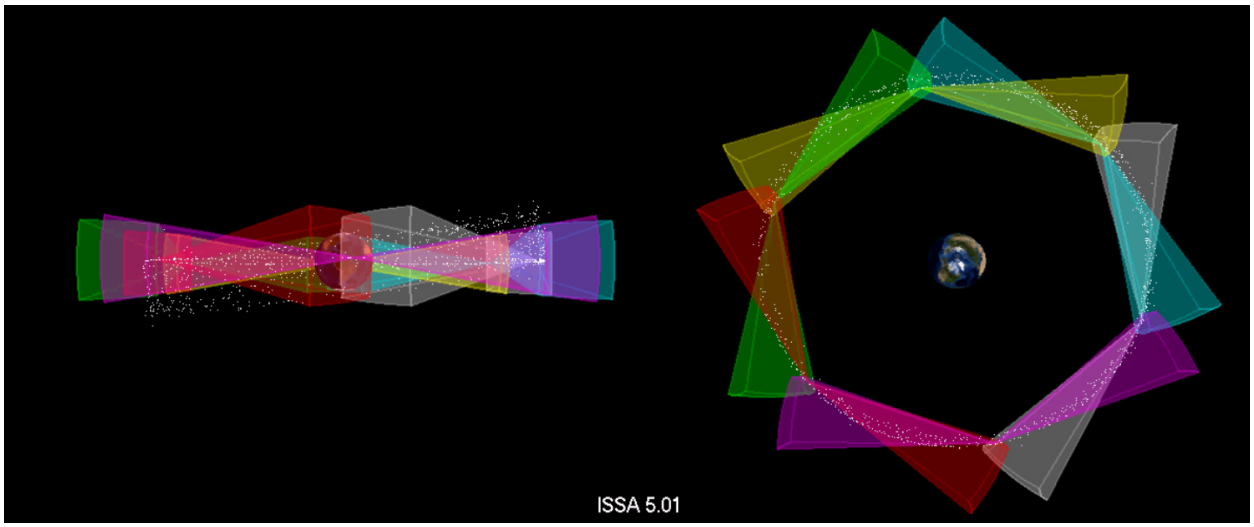

Figure 6 A notional commercially-hosted architecture using six hosts equally spaced 60° along the GEO belt. Each host has two telescopes with a 20° x 20° FOV, with the optical axis pointing 20° inward relative to the velocity/anti-velocity direction. The positions of GEO space objects from space-track.org are shown.

Figure 6 also illustrates another important geometric consideration—whether or not the sensor is able to see the apparent NS "turn around" point for objects, or when θ_{DEC} = inclination. The significance of this consideration is the detection sensitivity, or naturally taking advantage of when the relative motion is minimized. The absolute altitude above and below the GEO belt for the "turn around" points is $a_{GEO} \cdot inclination$, or for a 15° inclined object, approximately 11,000 km. When viewed from 60° away in the GEO belt, or at a range of ~42,000 km, this 11,000 km equals an angle of ~14.7°, or insufficient for the proposed 20° FOV system which only has 10° above/below the GEO belt. One potential approach is to offset the sensors in either the north or south direction, so that a larger volume of the turn-around points may be sampled every 24 hours.

Another potential trade or augmentation is to place another pair of secondary sensors mated with the first. The orientation proposed for the notional architecture provides no coverage along the velocity and anti-velocity

direction. A much smaller aperture could be used to provide this coverage, as the ranges of interest aren't as significant.

Finally, when examining the field of view and the ranges involved, high angular rates for objects will be experienced for the closer ranges, while lower rates for the farther ranges. For the particular proposal above, the edge of the FOV closest to GEO (farthest from Earth) will be seeing objects that are only 20° away in GEO, while the edge of the FOV farthest away from the velocity vector (closest to Earth) will be seeing objects that are 60° away in GEO. Assuming the detected objects are in the GEO orbit, those on one side of the image will have angular rates some 3x higher than those on the other side. One means of maximizing sensitivity is to tailor the integration time across the focal plane, consistent with the distances to the anticipated GEO objects.

6 A PLAUSIBLE FUTURE?

It would seem the time is right to reconsider commercially-hosted payloads for SSA. They satisfy several objectives of the US National Space Policy and National Security Space Strategy, to include improved resiliency and a means to "detect, identify, and attribute actions in space that are contrary to responsible use". Furthermore, declining US defense budgets warrant examination of such approaches. The technical performance of such payloads is significant, in particular when the solar phase angle diversity is considered along with the alternate viewing geometry for improving initial orbit determination estimates, and updating existing orbits. The small object sizes accessible with such systems would provide a better understanding of the small size GEO debris population, which in turn informs improved debris mitigation practices and preservation of the GEO environment.

Acknowledgement: The author greatly appreciates the contributions of Marc Herklotz, Marlyn Evenson and Maj. Steven Brune for the Integrated Space Situational Awareness (ISSA) modeling work illustrating the proposed sensor architecture.

Disclaimer: The views expressed in this document are those of the author and do not reflect the official policy or position of the U. S. Air Force, Department of Defense, or the U. S. Government.

7 REFERENCES

[1] National Space Policy of the United States of America, http://www.whitehouse.gov/sites/default/files/national_space_policy_6-28-10.pdf (accessed 25 August 2011).

[2] National Security Space Strategy, Unclassified Summary, http://www.defense.gov/home/features/2011/0111_nsss/docs/NationalSecuritySpaceStrategyUnclassifiedSummary_Jan2011.pdf (accessed 25 Aug 2011)

[3] Timothy L. Deaver, "Leveraging Commercial Communication Satellites to support the Space Situational Awareness Mission Area," in *Advanced Maui Optical and Space Surveillance Technologies Conference*, 2008, pp. 69-74.

[4] Hosted Payloads web site http://www.hostedpayload.com/ and Hosted Payload Alliance site http://hostedpayloadalliance.org/

[5] Inter-Agency Space Debris Coordination Committee (IADC) Space Debris Mitigation Guidelines, IADC-02-01, Revision 1, September 2007. (http://www.iadc-online.org/Documents/Docu/IADC_Mitigation_Guidelines_Rev1_Sep07.pdf, accessed 25 August 2011)

[6] Jonathan D. Lowe, David A. Vallado and Bob Hall, "Technical analysis of commercially hosted optical payloads for enhanced SSA," *2010 Advanced Maui and Optical Space Surveillance Technologies Conference*, pp. 637-645.

[7] T. Schildknecht, U. Hugentobler, and M. Ploner, "First GEO Survey Test Observations with the ESA 1 m Telescope in Tenerife," *Proceedings of the 2000 Space Control Conference*, Lincoln Laboratory Project Report Project Report STK-25, pp. 73-79.

[8] Nicholas L. Johnson, "Orbital Debris: The Growing Threat to Space Operations," *33rd Annual AAS Guidance and Control Conference*, February 2010, AAS 10-011.

[9] T. Schildknecht, et al, "Optical Observations of Space debris in High-Altitude Orbits," *Proceedings of the Fourth European Conference on Space Debris*, August 2005, ESA SP-587.

[10] T. Schildknecht, et al, "AIUB Efforts to Survey, Track and Characterize Small-Size Objects," *2010 Advanced Maui and Optical Space Surveillance Technologies Conference*, pp. 8-14.

[11] G. Drolshagen, T. Nehls and R. Noomen, "The Small Size Debris Population in the GEO Belt," *Proceedings of the Fifth European Conference on Space Debris*, July 2009, ESA SP-672.

[12] Mark Bolden, Paul Sydney, Paul Kervin, "Pan-STARRRS status and Geo Observations Results," *2011 Advanced Maui and Optical Space Surveillance Technologies Conference*.

[13] Darren S. McKnight and Frank R. Di Pentino, "New Insights on the Orbital Debris Collision Hazard at GEO," *62nd International Astronautical Congress*, Capetown, South Africa, 2011.

[14] Swiss Re, "Space Debris: On a Collision Course for Insurers?", http://media.swissre.com/documents/Publ11_Space+debris.pdf (accessed 25 August 2011).

[15] William E. Krag, "Visible Magnitude of Typical Satellites in Synchronous Orbits," Massachusetts Institute of Technology, September 6, 1974, ESD-TR-74-278.

[16] James R. Shell, "Optimizing Orbital Debris Monitoring with Optical Telescopes," *2010 Advanced Maui and Optical Space Surveillance Technologies Conference*, pp. 427-443.